Light-Triggered Theranostics Based on Photosensitizer-Conjugated Carbon Dots for Simultaneous Enhanced-Fluorescence Imaging and Photodynamic Therapy

Peng Huang,
Institute of Micro-Nano Science and Technology, Shanghai Jiao Tong University, 800 Dongchuan Road, Shanghai 200240, PR China

Laboratory of Molecular Imaging and Nanomedicine (LOMIN), National Institute of Biomedical Imaging and Bioengineering (NIBIB), National Institutes of Health, 31 Center Dr, Suite 1C14, Bethesda, MD 20892-2281, USA

Jing Lin,
Institute of Micro-Nano Science and Technology, Shanghai Jiao Tong University, 800 Dongchuan Road, Shanghai 200240, PR China

Xiansong Wang,
Institute of Micro-Nano Science and Technology, Shanghai Jiao Tong University, 800 Dongchuan Road, Shanghai 200240, PR China

Zhe Wang,
Laboratory of Molecular Imaging and Nanomedicine (LOMIN), National Institute of Biomedical Imaging and Bioengineering (NIBIB), National Institutes of Health, 31 Center Dr, Suite 1C14, Bethesda, MD 20892-2281, USA

Chunlei Zhang,
Institute of Micro-Nano Science and Technology, Shanghai Jiao Tong University, 800 Dongchuan Road, Shanghai 200240, PR China

Meng He,
Institute of Micro-Nano Science and Technology, Shanghai Jiao Tong University, 800 Dongchuan Road, Shanghai 200240, PR China

Qin Wang,
Institute of Micro-Nano Science and Technology, Shanghai Jiao Tong University, 800 Dongchuan Road, Shanghai 200240, PR China

Feng Chen,
Institute of Micro-Nano Science and Technology, Shanghai Jiao Tong University, 800 Dongchuan Road, Shanghai 200240, PR China

Zhiming Li,
Institute of Micro-Nano Science and Technology, Shanghai Jiao Tong University, 800 Dongchuan Road, Shanghai 200240, PR China

Guangxia Shen,
Institute of Micro-Nano Science and Technology, Shanghai Jiao Tong University, 800 Dongchuan Road, Shanghai 200240, PR China

Correspondence to: Guangxia Shen, gxshen@sjtu.edu.cn; Daxiang Cui, dxcui@sjtu.edu.cn; Xiaoyuan Chen, shawn.chen@nih.gov.

Daxiang Cui, and
Institute of Micro-Nano Science and Technology, Shanghai Jiao Tong University, 800 Dongchuan Road, Shanghai 200240, PR China

Xiaoyuan Chen
Laboratory of Molecular Imaging and Nanomedicine (LOMIN), National Institute of Biomedical Imaging and Bioengineering (NIBIB), National Institutes of Health, 31 Center Dr, Suite 1C14, Bethesda, MD 20892-2281, USA

Center for Molecular Imaging and Translational Medicine, School of Public Health, Xiamen University, Xiamen 361005, China

Guangxia Shen: gxshen@sjtu.edu.cn; Daxiang Cui: dxcui@sjtu.edu.cn; Xiaoyuan Chen: shawn.chen@nih.gov

Keywords

Theranostics; carbon dots; chlorin e6 (Ce6); fluorescence imaging; photodynamic therapy

Theranostics, combining both medical diagnostics and therapeutics to achieve an optimizing efficacy and safety of comprehensive regime, is an emerging interdiscipline that is paving the avenue towards the goal of personalized medicine.[1] Activatable theranostic agents can enhance the selectivity and specificity for disease destruction with high localized cytotoxicity and little collateral damage.[2] So far, controllable activation by an external stimulus such as temperature, pH, applied magnetic or electrical field, ultrasound, light, or enzymatic action have been proposed as triggered delivery systems.[3] Over the past decade, light-triggered theranostics, such as photodynamic-, photothermal- and photo-triggered chemotherapy have received increased attention due to the advantage of highly specific spatial and temporal control of compound release.[4] The theranostic constructs could advance a novel category of clinical solution which possesses early recognition of the disease by enhancing contrast in various imaging modalities followed by the tailored guidance of therapy.

Photodynamic therapy (PDT) is an extraordinary theranostic modality for a number of malignant and nonmalignant diseases.[5] The general procedure of PDT involves the systemic, local, or topical administration of a non-toxic drug or dye known as a photosensitizer (PS) followed by selective illumination with appropriate wavelength and power of light.[2e, 6] In the presence of oxygen, PS can transfer the absorbed photon energy to surrounding oxygen molecules, generating reactive oxygen species (ROS) including singlet oxygen (SO) or free radicals and consequently causing cell death and tissue destruction. Meanwhile, upon light activation, PS can emit fluorescence due to the relaxation of the excited-singlet-state PS back to the ground state.[1e] The emitted fluorescence can be employed for locating diseases, photodiagnosis and molecular imaging, which is known as photosensitizer fluorescence detection (PFD).[4a, 7] Therefore, organic fusion of PFD and PDT enables online imaging of drug for the detection of disease, image-guided drug delivery and treatments, guidance of surgical resection, and monitoring of treatment response.[8]

Unfortunately, PFD has certain limitations that are similar to any fluorescence-imaging based detection strategy, because the PS generally was excited by blue or UV light that shows very limited penetration depth about a few hundred micrometers. For flat lesions, such as carcinomas in situ, this approach is highly successful at delineating disease margins, while lesions which may have a considerable subsurface cannot be observed without depth-resolved imaging. There are three approaches to address those inherent limitations: (1) to enhance the fluorescence of PS; (2) to develop novel PS with long excitation wavelength;

(3) to implement of a multimodality imaging approach based on PFD for identification of neoplastic regions that is complemented by a depth-resolved structural imaging modality.

An ideal theranostic PS is an agent that has high SO quantum yield (QY) for PDT and also a reasonably high fluorescence QY for PFD.[9] Unfortunately, even the most successful PSs, such as Photolon®, Fotolon®, and Tookad®, bear lower fluorescence QY than traditional fluorescent dyes, thus limiting the theranostic use for simultaneous PFD and PDT.[1e] To address this issue, quantum dots (QDs) were employed for improved PFD and PDT by two different excitation pathways: (1) indirect excitation by Förster (fluorescence) resonance energy transfer (FRET) from the nanocrystals to PSs; (2) direct excitation of the PS.[10] However, most traditional QDs contain heavy metal elements (such as Cd^{2+}, Pb^{2+}, etc.). The cytotoxicity of the released heavy metal ions in biological systems and potential environmental hazard of these ions limit further applications of QDs in theranostics.[11]

Carbon dots (C-dots), a very recent rising star, as a class of zero-dimensional carbon nanomaterials possess, some of the same major advantageous characteristics of QDs, such as high photostability, tunable emission, and large two-photon excitation cross-sections.[12] Moreover, C-dots exhibit nonblinking fluorescence, excellent water solubility, and are cheaply produced.[13] Particularly, C-dots without heavy metal content are more environmentally friendly and can be much safer for biological applications.[14] Herein, we strategically designed and prepared novel multifunctional chlorin e6-conjugated C-dots (C-dots-Ce6) as the light-triggered theranostics for simultaneous enhanced-PFD and PDT by FRET mechanism.

The synthetic scheme for making C-dots-Ce6 is shown in Figure S1. Scheme 1 illustrates the FRET process between C-dots and Ce6. The C-dots with PEG diamine, PEG2000N as the surface passivation agent were prepared and characterized as previously reported.[12b, 12c] PEG-coated C-dots (C-dots-NH$_2$) were terminated with amine groups. Covalent binding of Ce6 to the C-dots-NH$_2$ was performed using a modified EDC–NHS reaction as described by Jönsson et al.[15] C-dots were employed for improved PFD and PDT by two different excitation pathways: (1) indirect excitation by FRET from the C-dots to Ce6; (2) direct excitation of the Ce6.

The size and morphology of as-prepared C-dots-Ce6 was characterized by atomic force microscopy (AFM) (Figure 1). Figure 1A shows the AFM image of original C-dots as spherical nanoparticles with diameters in the range of 1~2 nm (determined by AFM measured height). After PEG passivation, the C-dots-NH$_2$ was characterized by transmission electronic microscopy (TEM). Figure S2A shows the TEM image of C-dots-NH$_2$. As can be seen, the PEG-coated C-dots are spherical nanoparticles with an average size of 2.23 ± 0.37 nm, which was confirmed by a detailed analysis of the particle size of around 200 nanoparticles (see Figure S2B). After conjugation with Ce6, the size of C-dots-Ce6 is in the range of 2.5–10 nm (Figure 1B). The C-dots-Ce6 is stable in various media such as deionized distilled water, PBS buffer (pH 7.4), saline and serum (see inset).

Regarding the photophysical and photochemical properties of C-dots-Ce6, optical absorption and fluorescence spectroscopies were used to investigate the binding of Ce6 to C-dots. Figure 2A shows the UV-vis absorbance spectra of C-dots-NH$_2$, Ce6 and C-dots-Ce6. The Ce6 exhibits a strong Soret absorption at 406 nm, and weak Q-bands between 500 and 700 nm. C-dots-NH$_2$ without Ce6 show virtually no absorption in the range of 400~800 nm. After conjugation with Ce6, the absorption of C-dots-Ce6 is similar to that of Ce6, indicating no changes in the Ce6 chromophore upon conjugation. The conjugation efficiency of Ce6 was calculated by using Ce6 UV calibration curve at 663 nm. The standard curve had a good linear relationship, described by the following typical equation:

Y=0.07712+27.86047× (R^2=0.9948).[2e, 3k] The conjugation efficiency was ~50% estimated by the typical equation, based on the added Ce6.

The fluorescence emission spectra of C-dots showed shifted emission peaks from 473 nm to 525 nm as the excitation wavelength was changed from 400 nm to 480 nm (see Figure S2C and D). The inset in Figure S2D shows the fluorescence image of C-dots dispersed in PBS buffer (pH 7.4) under the excitation at 430 nm. The C-dots display a green fluorescence signal, which is attributed to the poly-aromatic sp^2 carbon nanostructures in the C-dots, as well as the various surface functional groups on the nanoparticles.[12a] Figure 2B represents the fluorescence emission spectra and images of the samples in PBS buffer (pH 7.4). The excitation wavelength is fixed at 430 nm, which is in accordance with the condition used for *in vivo* imaging. The C-dots exhibit a fluorescence peak centered at 525 nm, which is near the Q-band absorption of Ce6 at 503 nm. The fluorescence emission of C-dots in the range of 450–650 nm overlaps with the absorption of Ce6 at the same range (see Figure S3). Therefore, the fluorescence emission of C-dots can be used to excitate Ce6 indirectly. C-dots-Ce6 shows a remarkably stronger fluorescence (~35-fold) in PBS than free Ce6, at the same concentration of Ce6 (76 μM). For comparison purpose, the fluorescence of C-dots-Ce6 was also detected by excitation at 430 nm and 510 nm, respectively (Figure S4). It indicated that the fluorescence of C-dots-Ce6 upon 430 nm excitation is remarkably stronger than that of C-dots-Ce6 upon 510 nm excitation, which suggests that FRET is weak upon 510 nm excitation. The enhancement of Ce6 fluorescence QY is due to the following reasons: (1) indirect excitation through FRET from C-dots to Ce6; (2) Ce6 conjugated C-dots prevents Ce6 aggregation and improve the solubility of Ce6 in aqueous solution. In addition, the maximum emission of C-dots-Ce6 at ~668 nm is suitable for optical imaging of live animals. The above results permit the use of C-dots-Ce6 as fluorescent nanoprobes for *in vivo* imaging. The inset fluorescence images in Figure 2B indicate that the C-dots-Ce6 and C-dots display a red and green fluorescence signal, respectively. In Figure 2C, the FT-IR spectrum of C-dots-Ce6 is similar to that of Ce6, which suggests that Ce6 was successfully conjugated with the C-dots. Zeta potentials of C-dots, C-dots-NH$_2$ and C-dots-Ce6 were recorded at pH 7.0 as shown in Figure 2D. The zeta potential of C-dots is −23.85 ± 2.89, due to the existence of –OH/-COOH groups on the surface of C-dots. After passivation with PEG diamine, the zeta potential of C-dots-NH$_2$ is −9.38 ± 1.10. After conjugation with Ce6, the zeta potential of C-dots-Ce6 turns into −31.92 ± 1.01. The samples all bear negative charges, which may be responsible for the high water dispersity and solubility of the as-prepared particles.

The generation of SO by C-dots-Ce6 was detected chemically using the singlet oxygen sensor green (SOSG) as a detector. For SOSG detector, intramolecular electron transfer (ET) quenches the fluorescence from the light-emitting chromophore before the reaction with SO. After reaction with SO, with the formation of the endoperoxide, the electron transfer is prohibited, and fluorescence is recovered.[16] Figure 3A and B show the decrease in optical density (OD) at 256, 402, and 653 nm as the function of irradiation time. In Figure 3C, the SOSG's fluorescence intensity exhibit a time-dependent enhancement after reaction with SO, generated from C-dots-Ce6 upon irradiation. Figure 3D shows the increase in fluorescence intensity at the special peak of SOSG (530 nm) as a function of laser irradiation time. For SOSG alone with laser irradiation group, the fluorescence intensity is a constant. For pure C-dots with laser irradiation group, the fluorescence intensity is also a constant, which indicates that pure C-dots alone cannot generate SO. Compared with Ce6 with laser irradiation group, the increase of SOSG's fluorescence intensity is lower than the increase in C-dots-Ce6 with laser irradiation group, which suggests that the C-dots can enhance the efficiency of SO production of Ce6 on C-dots-Ce6. Meanwhile, the results indicate that the SO can be produced by Ce6 after conjugation with C-dots. Therefore, the C-dots-Ce6 could be used for *in vivo* tumor PDT treatment.

To determine the cellular localization of C-dots-Ce6, fluorescence imaging was performed on human MGC803 cells using an upright Olympus IX71 optical microscope integrated with a CRi Nuance multispectral imaging system (Cambridge Research & Instrumentation, Inc., Woburn, MA, USA). At 2 h after incubation with 10 μM C-dots-Ce6, cells displayed an intense homogeneous cytoplasmic red fluorescence around nuclei, indicating accumulation of C-dots-Ce6 in cells (Figure 4A–C). DAPI (4',6-diamidino-2-phenylindole) staining was used to visualize nuclei (Figure S5). In Figure S5D, the blue fluorescence representing the nuclei stained by DAPI are surrounded by red fluorescence suggesting internaalization of C-dots-Ce6 into the cytoplasm. As PDT effect is dependent on the uptake of photosensitizers by tumor cells, the strong fluorescence intensity of intracellular C-dots-Ce6 predicts available PDT effects.[3i, 3k] For comparison purpose, cellular localization of C-dots-NH$_2$ was shown in Figure S6. The cells incubated with C-dots-NH$_2$ displayed green fluorescence signal in the cytoplasm. The fluorescence emission spectrum of C-dots-Ce6 in the cells was recorded using CRi Nuance multi-spectral imaging system (Figure S7). The C-dots-Ce6 has two characteristic peaks, a maximum at ~670 nm, which is attributed to Ce6, and a shoulder at ~530 nm, which is attributed to C-dots. The results are consistent with those recorded on fluorescence spectroscopy.

PDT effect of C-dots-Ce6 in the concentration range of 0~50 μM on MGC803 cells was detected by CCK-8 assay. Cell viability was normalized to control cells (no drug and nonirradiated). Exposure of tumor cells to C-dots-Ce6 for 24 h followed by laser irradiation induced a concentration-dependent cytotoxicity to MGC-803 cells, which was significantly different from nonirradiated controls and Ce6 alone controls as shown in Figure 4D. With the increase of drug concentration, the cell viability gradually decreased. The cells treated with C-dots-Ce6 without light exposure displayed over 90% cell viability, suggesting that C-dots-Ce6 alone had no adverse effect on tumor cells. Interestingly, the PDT effect of C-dots-Ce6 is stronger than the effect of Ce6 alone, which suggests that C-dots-Ce6 is advantageous over the conventional formulation, which is attributed to the enhanced efficiency of SO production of Ce6 by C-dots. Laser-triggered PDT effect of C-dots-Ce6 was also observed using trypan blue staining. As shown in Figure 4E, on the boundary of laser spot, cells without irradiation displayed good physiological state with spindle morphology. However, all the cells were killed and displayed a blue color on the laser spot in Figure 4F. These results were in good accordance with the SO generation data, further confirming the potential of C-dots-Ce6 for destroying tumor cells by light irradiation. From the corresponding fluorescence image (Figure S8), there is still an intense homogeneous red signal around the nucleolus, indicating the most PS molecules are remained after irradiation. Obviously, the C-dots-Ce6 can meet the requirements of repeated irradiation treatment after injection.

To demonstrate the feasibility of C-dots-Ce6 for *in vivo* fluorescence imaging, 100 μL of C-dots-Ce6 (100 μM) was injected into the left rear flank area of mice. Then the fluorescence images of mice were recorded on a Carestream Molecular Imaging In-Vivo MS FX PRO system. As shown in Figure S9, the subcutaneous injection site displayed a strong fluorescence signal. With time, the area of the fluorescence signal kept expanding from center, which suggests that C-dots-Ce6 has good distribution ability in tissue. It can be attributed to its good stability and dispersibility in aqueous systems. The results indicate that C-dots-Ce6 can be used as an ideal fluorescence agent for imaging-guided *in vivo* PDT treatment.

To further demonstrate the ability of C-dots-Ce6 as *in vivo* theranostics, we investigated its feasibility for fluorescence imaging-guided PDT. Nude Mice with subcutaneous MGC803 gastric cancer xenograft were selected as the animal model. When the tumors reached 25~30 mm^3, the mice were treated with intravenous injection of C-dots-Ce6 (5 μmol equevalent of

Ce6/kg body weight). The nude mice without injection of C-dots-Ce6 were selected as the control. NIR fluorescence imaging was employed to monitor PDT *in vivo*. As shown in Figure 5A, after injection, significant fluorescence emitted from the C-dots-Ce6 injected mice was observed in the tumor area. Meanwhile, there are also fluorescence signal in the other tissues. At 24 h time point, the organs of C-dots-Ce6 injected mice were harvested for *ex vivo* imaging to quantify tissue/organ distribution (Figure 5B). The strong fluorescence signal displayed in the kindeys suggest that the C-dots-Ce6 can be excreted from the body by renal clearance. The fluorescence intensity of organs were quantified in Figure S10. It can be estimated that the accumulation of C-dots-Ce6 on tumor tissue is ~21.1 %ID/g.

C-dots-Ce6 accumulation in the tumor was quantified by identifying the tumor as a region of interest to measure its Ce6 fluorescence intensity (Figure 5C). The average fluorescence intensity from Ce6 acquired in the tumor areas quickly arose within 2~4 h post-injection and reached a plateau in 4~8 h post-injection followed by steady decrease over time (n = 5). According to the observation from NIR fluorescence imaging, 8 h was selected as the suitable time point to implement PDT. The tumor area was irradiated for 10 min using a 671 nm laser (100 mW/cm^2). The C-dots-Ce6 administration/irradiation group showed partial tumor regression as illustrated in Figure 5D. These results indicate that C-dots-Ce6 has excellent imaging and tumor-homing ability without compromising the photodynamic efficacy, and is suitable for simultaneous PFD and PDT of tumor in vivo.

C-dots as the carrier to load PSs or dyes have the following advantages: (1) C-dots can prevent aggregation of PSs or dyes and improve the stability and solubility of PSs or dyes in aqueous/biological media; (2) C-dots can improve the biocompatibility of the complex and lower the cytotoxicity of PSs or dyes; (3) C-dots can prolong the circulation half-life of PSs or dyes in the bloodstream and permeate barriers more rapidly including cell membranes and fenestrated vasculature in the cancer area; (4) C-dots can enhance the tumor-homing ability of PSs or dyes based on the enhanced permeability and retention (EPR) effect and increase the ingestion of tumor tissue; (5) C-dots can indirectly excite the PSs or dyes by FRET mechanism.

In summary, a novel theranostic platform based on photosensitizer-conjugated carbon dots is successfully designed and developed. We have demonstrated that C-dots-Ce6 is a good candidate with excellent imaging and tumor-homing ability for NIR fluorescence imaging guided PDT treatment. The prepared C-dots-Ce6 owns good stability and high water dispersibility and solubility, noncytotoxicity, good biocompatibility, enhanced photosensitizer fluorescence detection and remarkable photodynamic efficacy upon irradiation. Our results indicated that the synthesized multifunctional nanocarrier platform is effective for simultaneous enhanced-PFD and PDT of gastric cancer tumor *in vivo*. It may have great potential for applications in the clinic to treat patients with gastric cancer or other tumors in the near future.

Supplementary Material

Refer to Web version on PubMed Central for supplementary material.

Acknowledgments

References

1. a) Ng KK, Lovell JF, Zheng G. Acc. Chem. Res. 2011; 44:1105. [PubMed: 21557543] b) Lovell J, Jin C, Huynh E, Jin H, Kim C, Rubinstein J, Chan W, Cao W, Wang L, Zheng G. Nat. Mater. 2011; 20:324. [PubMed: 21423187] c) Shi J, Liu TWB, Chen J, Green D, Jaffray D, Wilson BC, Wang F, Zheng G. Theranostics. 2011; 1:363. [PubMed: 21938264] d) Chen XS. Theranostics. 2011; 1:1. [PubMed: 21547150] e) Rai P, Mallidi S, Zheng X, Rahmanzadeh R, Mir Y, Elrington S, Khurshid A, Hasan T. Adv. Drug Deliv. Rev. 2010; 62:1094. [PubMed: 20858520] f) Xie J, Liu G, Eden H, Ai H, Chen X. Acc. Chem. Res. 2011; 44:883. [PubMed: 21548618] g) Xie J, Lee S, Chen X. Adv. Drug Deliv. Rev. 2010; 62:1064. [PubMed: 20691229] h) Jiang X, Sha X, Xin H, Chen L, Gao X, Wang X, Law K, Gu J, Chen Y, Jiang Y. Biomaterials. 2011; 32:9457. [PubMed: 21911250] i) Chen F, Huang P, Zhu YJ, Wu J, Zhang CL, Cui DX. Biomaterials. 2011; 32:9031. [PubMed: 21875748] j) Chen XS. Theranostics. 2012; 2:1. [PubMed: 22272216]

2. a) Lovell J, Liu T, Chen J, Zheng G. Chem. Rev. 2010; 110:2839. [PubMed: 20104890] b) Yu MK, Park J, Jon S. Theranostics. 2012; 2:3. [PubMed: 22272217] c) Liu TWB, Chen J, Burgess L, Cao W, Shi J, Wilson BC, Zheng G. Theranostics. 2011; 1:354. [PubMed: 21938263] d) Jang B, Choi Y. Theranostics. 2012; 2:190. [PubMed: 22375157] e) Huang P, Xu C, Lin J, Wang C, Wang X, Zhang C, Zhou X, Guo S, Cui D. Theranostics. 2011; 1:240. [PubMed: 21562631] f) Jeong H, Huh M, Lee SJ, Koo H, Kwon IC, Jeong SY, Kim K. Theranostics. 2011; 1:230. [PubMed: 21562630]

3. a) Du J, O'Reilly RK. Soft Matter. 2009; 5:3544.b) Du J, O'Reilly R. Chem. Soc. Rev. 2011; 40:2402. [PubMed: 21384028] c) Lovell JF, Jin CS, Huynh E, MacDonald TD, Cao W, Zheng G. Angew. Chem. Int. Ed. 2012; 51:2429.d) Cai X, Yang F, Gu N. Theranostics. 2012; 2:103. [PubMed: 22287990] e) Yavuz MS, Cheng Y, Chen J, Cobley CM, Zhang Q, Rycenga M, Xie J, Kim C, Song KH, Schwartz AG. Nat. Mater. 2009; 8:935. [PubMed: 19881498] f) Li C, Zhang Y, Hu J, Cheng J, Liu S. Angew. Chem. Int. Ed. 2010; 49:5120.g) Chan JM, Zhang L, Tong R, Ghosh D, Gao W, Liao G, Yuet KP, Gray D, Rhee JW, Cheng J. Proc. Natl. Acad. Sci. USA. 2010; 107:2213. [PubMed: 20133865] h) Wang C, Tao H, Cheng L, Liu Z. Biomaterials. 2011; 32:6145. [PubMed: 21616529] i) Sun Y, Chen Z, Yang X, Huang P, Zhou X, Du X. Nanotechnology. 2009; 20:135102. [PubMed: 19420486] j) Li Z, Huang P, Zhang X, Lin J, Yang S, Liu B, Gao F, Xi P, Ren Q, Cui D. Mol. Pharm. 2009; 7:94. [PubMed: 19891496] k) Huang P, Li Z, Lin J, Yang D, Gao G, Xu C, Bao L, Zhang C, Wang K, Song H. Biomaterials. 2011; 32:3447. [PubMed: 21303717] l) Lee H, Lee S, Min KH, Kim MS, Lee DS, Choi Y, Kwon IC, Kim K, Jeong SY. Chem. Comm. 2010; 46:5668. [PubMed: 20623050] m) Chen Y, Liang G. Theranostics. 2012; 2:139. [PubMed: 22375155]

4. a) Celli JP, Spring BQ, Rizvi I, Evans CL, Samkoe KS, Verma S, Pogue BW, Hasan T. Chem. Rev. 2010; 110:2795. [PubMed: 20353192] b) Huang X, El-Sayed IH, Qian W, El-Sayed MA. J. Am. Chem. Soc. 2006; 128:2115. [PubMed: 16464114] c) Huang X, Jain P, El-Sayed I, El-Sayed M. Laser Med. Sci. 2008; 23:217.d) Luo Y, Shiao Y, Huang Y. ACS nano. 2011; 5:7796. [PubMed: 21942498] e) Tian B, Wang C, Zhang S, Feng L, Liu Z. ACS Nano. 2011; 5:7000. [PubMed: 21815655] f) Lee S, Ryu J, Park K, Lee A, Lee S, Youn I, Ahn C, Yoon S, Myung S, Moon D. Nano Lett. 2009; 9:4412. [PubMed: 19842672] g) Huang P, Bao L, Zhang C, Lin J, Luo T, Yang D, He M, Li Z, Gao G, Gao B. Biomaterials. 2011; 32:9796. [PubMed: 21917309] h) Cui D, Huang P, Zhang C, Ozkan CS, Pan B, Xu P. J. Control. Release. 2011; 152:e137. [PubMed: 22195805] i) Luo T, Huang P, Gao G, Shen G, Fu S, Cui D, Zhou C, Ren Q. Opt. Express. 2011; 19:17030. [PubMed: 21935063]

5. a) Huang Z, Xu H, Meyers AD, Musani AI, Wang L, Tagg R, Barqawi AB, Chen YK. Technol. Cancer Res. Treat. 2008; 7:309. [PubMed: 18642969] b) Huang Z, Li L, Wang H, Wang X, Yuan K, Meyers A, Yang L, Hetzel FW. J. Innov. Opt. Health Sci. 2009; 2:73.c) Park K, Lee S, Kang E, Kim K, Choi K, Kwon IC. Adv. Funct. Mater. 2009; 19:1553.

6. a) Chen ZL, Sun Y, Huang P, Yang XX, Zhou XP. Nanoscale Res. Lett. 2009; 4:400. [PubMed: 20596490] b) Liu F, Zhou X, Chen Z, Huang P, Wang X, Zhou Y. Mater. Lett. 2008; 62:2844.c) Huang P, Lin J, Yang D, Zhang C, Li Z, Cui D. J. Control. Release. 2011; 152:e33. [PubMed: 22195908]

7. a) Jeong H, Huh MS, Lee SJ, Koo H, Kwon IC, Jeong SY, Kim K. Theranostics. 2011; 1:230. [PubMed: 21562630] b) He X, Wu X, Wang K, Shi B, Hai L. Biomaterials. 2009; 30:5601. [PubMed: 19595455]

8. a) Liang X, Li X, Yue X, Dai Z. Angew. Chem. Int. Ed. 2011; 50:11622.b) Cheng Y, Meyers J, Broome A, Kenney M, Basilion J, Burda C. J. Am. Chem. Soc. 2011; 133:2583. [PubMed: 21294543]

9. a) Wang S, Gao R, Zhou F, Selke M. J. Mater. Chem. 2004; 14:487.b) Bechet D, Couleaud P, Frochot C, Viriot ML, Guillemin F, Barberi-Heyob M. Trends Biotechnol. 2008; 26:612. [PubMed: 18804298]

10. a) Juzenas P, Chen W, Sun YP, Coelho MAN, Generalov R, Generalova N, Christensen IL. Adv. Drug Deliv. Rev. 2008; 60:1600. [PubMed: 18840487] b) Samia A, Dayal S, Burda C. Photochem. Photobiol. 2006; 82:617. [PubMed: 16475871] c) Samia ACS, Chen X, Burda C. J. Am. Chem. Soc. 2003; 125:15736. [PubMed: 14677951] d) Juzenas P, Chen W, Sun YP, Coelho MAN, Generalov R, Generalova N, Christensen IL. Adv. Drug Deliv. Rev. 2008; 60:1600. [PubMed: 18840487] e) Yaghini E, Seifalian AM, MacRobert AJ. Nanomedicine. 2009; 4:353. [PubMed: 19331542] f) Tsay JM, Trzoss M, Shi L, Kong X, Selke M, Jung ME, Weiss S. J. Am. Chem. Soc. 2007; 129:6865. [PubMed: 17477530]

11. a) Huang P, Bao L, Yang D, Gao G, Lin J, Li Z, Zhang C, Cui D. Chem. Asian J. 2011; 6:1156. [PubMed: 21341374] b) Derfus AM, Chan WCW, Bhatia SN. Nano Lett. 2004; 4:11.c) Gao X, Cui Y, Levenson RM, Chung LWK, Nie S. Nat. Biotechnol. 2004; 22:969. [PubMed: 15258594] d) Cui D, Han Y, Li Z, Song H, Wang K, He R, Liu B, Liu H, Bao C, Huang P. Nano Biomed. Eng. 2009; 1:61.e) Li Z, Huang P, He R, Lin J, Yang S, Zhang X, Ren Q, Cui D. Mater. Lett. 2010; 64:375.f) Li Z, Huang P, Lin J, He R, Liu B, Zhang X, Yang S, Xi P, Ren Q. J. Nanosci. Nanotechnol. 2010; 10:4859. [PubMed: 21125820] g) Kim GB, Kim YP. Theranostics. 2012; 2:127. [PubMed: 22375154]

12. a) Sun YP, Zhou B, Lin Y, Wang W, Fernando KAS, Pathak P, Meziani MJ, Harruff BA, Wang X, Wang H. J. Am. Chem. Soc. 2006; 128:7756. [PubMed: 16771487] b) Cao L, Wang X, Meziani MJ, Lu F, Wang H, Luo PG, Lin Y, Harruff BA, Veca LM, Murray D. J. Am. Chem. Soc. 2007; 129:11318. [PubMed: 17722926] c) Yang ST, Cao L, Luo PG, Lu F, Wang X, Wang H, Meziani MJ, Liu Y, Qi G, Sun YP. J. Am. Chem. Soc. 2009; 131:11308. [PubMed: 19722643] d) Yang ST, Wang X, Wang H, Lu F, Luo PG, Cao L, Meziani MJ, Liu JH, Liu Y, Chen M. J. Phys. Chem. C. 2009; 113:18110.e) Wang X, Cao L, Yang ST, Lu F, Meziani MJ, Tian L, Sun KW, Bloodgood MA, Sun YP. Angew. Chem. Int. Ed. 2010; 122:5438.f) Wang F, Xie Z, Zhang H, Liu C, Zhang Y. Adv. Funct. Mater. 2011; 21:1027.g) Cao L, Yang ST, Wang X, Luo PG, Liu JH, Sahu S, Liu Y, Sun YP. Theranostics. 2012; 2:295. [PubMed: 22448196] h) Liu Z, Liang XJ. Theranostics. 2012; 2:235. [PubMed: 22448193]

13. a) Zhu H, Wang X, Li Y, Wang Z, Yang F, Yang X. Chem. Comm. 2009:5118. [PubMed: 20448965] b) Liu R, Wu D, Liu S, Koynov K, Knoll W, Li Q. Angew. Chem. Int. Ed. 2009; 121:4668.c) Tao H, Yang K, Ma Z, Wan J, Zhang Y, Kang Z, Liu Z. Small. 2011; 8:281.

14. a) Cao L, Yang ST, Wang X, Luo PG, Liu JH, Sahu S, Liu Y, Sun YP. Theranostics. 2012; 2:295. [PubMed: 22448196] b) Anilkumar P, Wang X, Cao L, Sahu S, Liu JH, Wang P, Korch K, Tackett KN II, Parenzan A, Sun YP. Nanoscale. 2011; 3:2023. [PubMed: 21350751]

15. Johnsson B, Löfås S, Lindquist G. Anal. Biochem. 1991; 198:268. [PubMed: 1724720]

16. a) Flors C, Fryer MJ, Waring J, Reeder B, Bechtold U, Mullineaux PM, Nonell S, Wilson MT, Baker NR. J. Exp. Bot. 2006; 57:1725. [PubMed: 16595576] b) Li B, Lin H, Chen D, Wang M, Xie S. Chin. Opt. Lett. 2010; 8:86.c) Zhu Z, Tang Z, Phillips JA, Yang R, Wang H, Tan W. J. Am. Chem. Soc. 2008; 130:10856. [PubMed: 18661988]
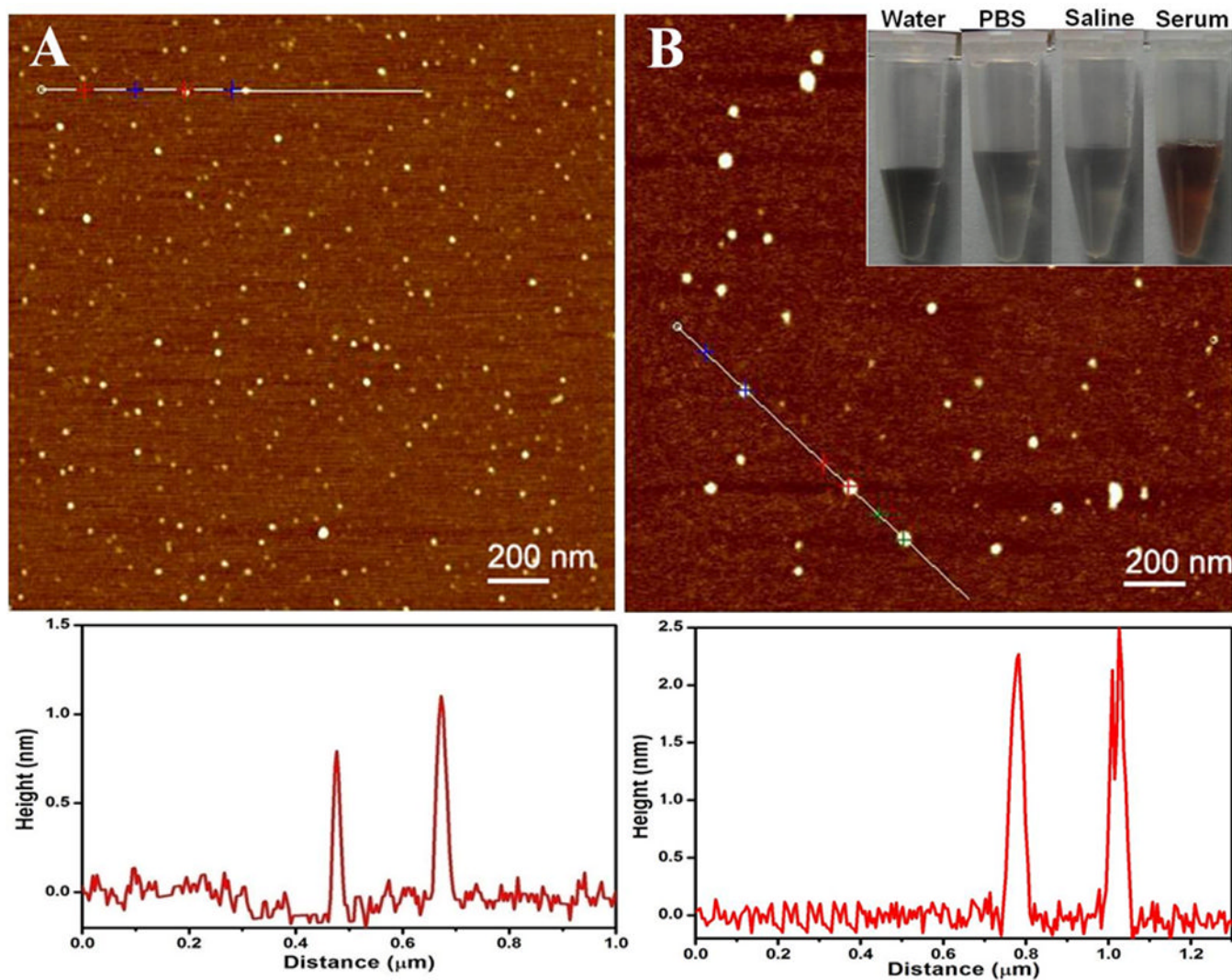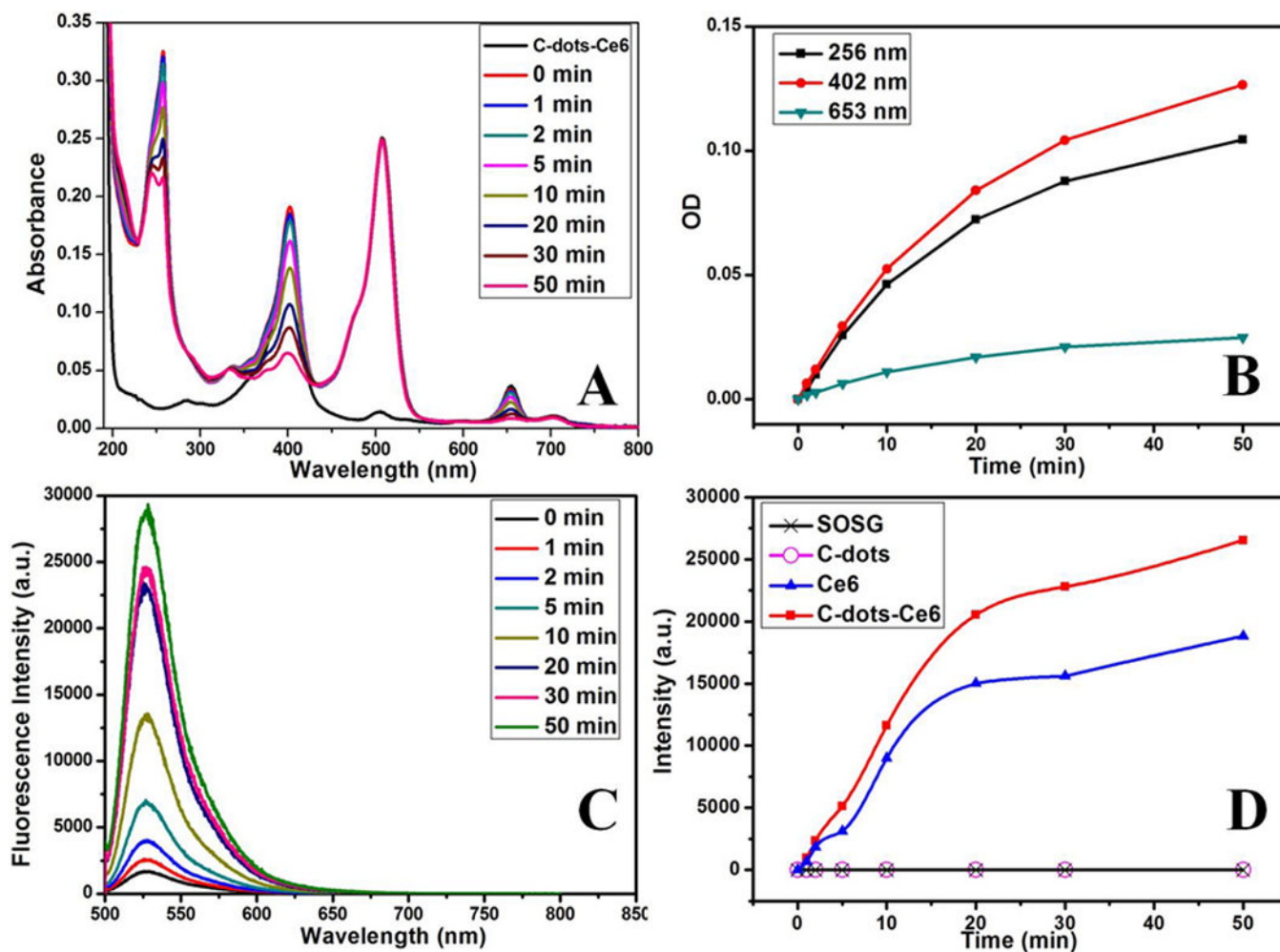
Figure 1.
(A) AFM topography image of C-dots on mica substrate, with the height profile along the line in the image. (B) AFM topography image of C-dots-Ce6 on mica substrate, with the height profile along the line in the image (The inset is the photographs of C-dots-Ce6 in different solutions such as deionized distilled water, PBS buffer (pH 7.4), saline and serum).
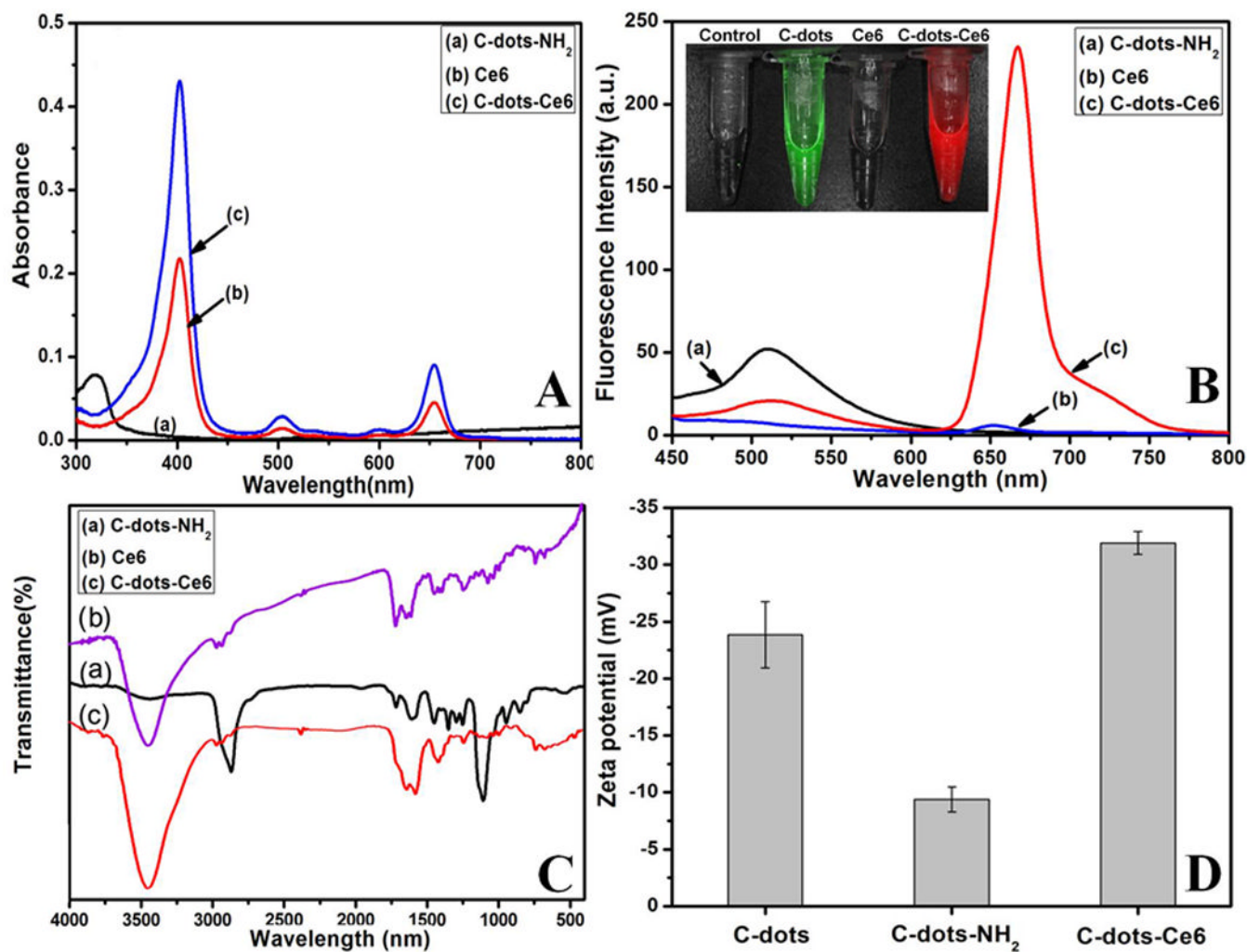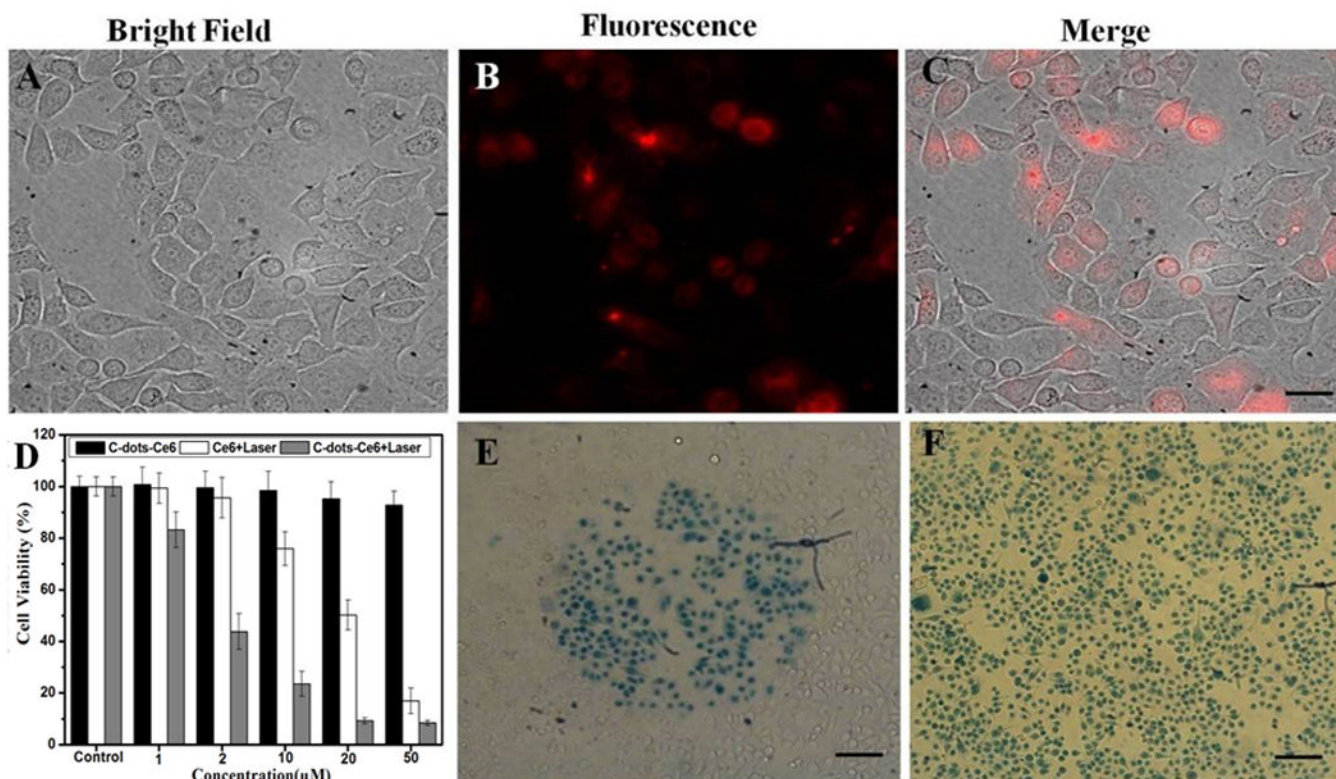
Figure 2.
(A) UV-vis absorbance spectra, (B) fluorescence emission spectra, and (C) FT-IR spectra of C-dots-NH_2 (a), Ce6 (b) and C-dots-Ce6 (c); (D) zeta potential of C-dots (a), C-dots-NH_2 (b) and C-dots-Ce6 (c). The same concentrations of Ce6 and C-dots-Ce6 (76 μM) were used for fluorescence detection.
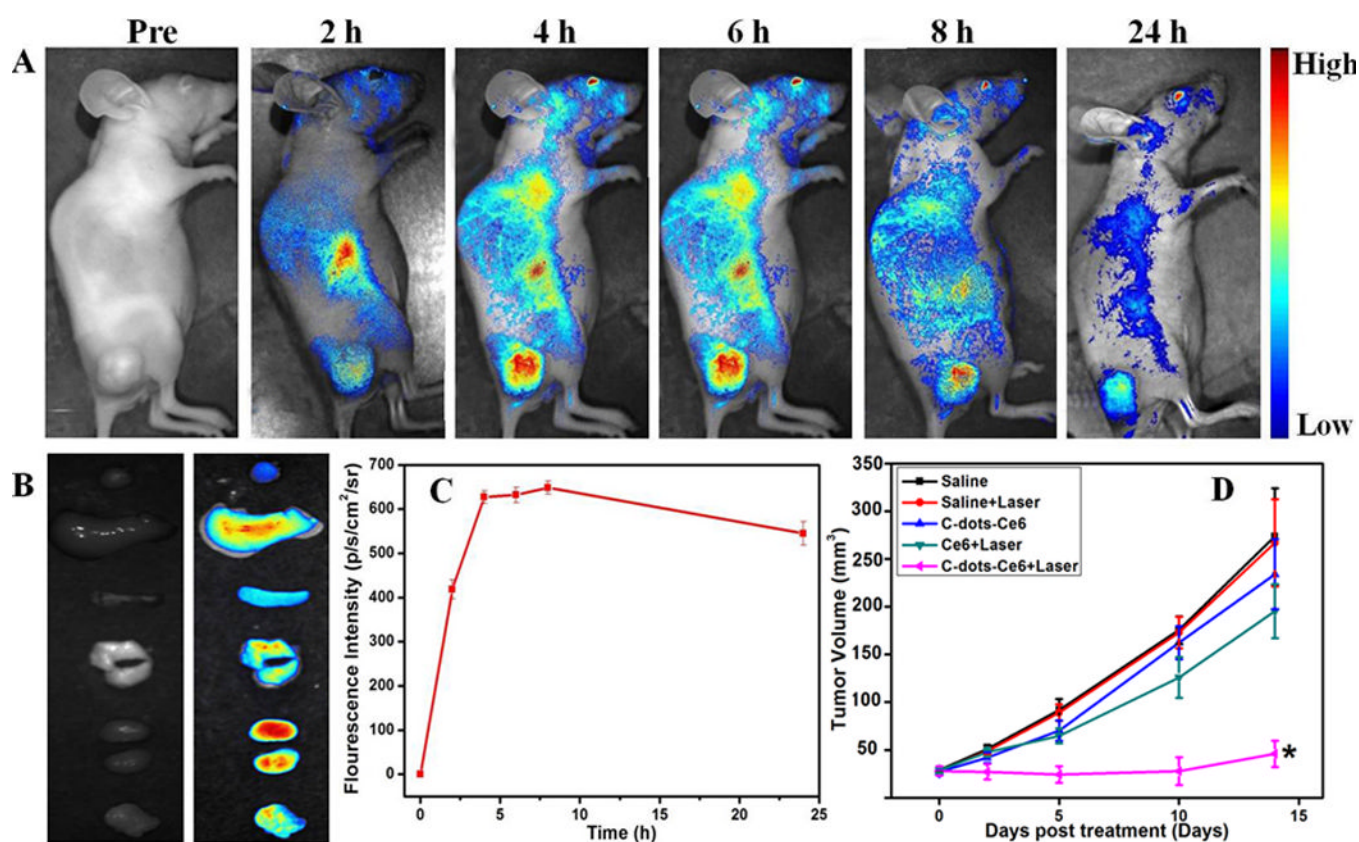
Figure 3.
(A) Time-dependent bleaching of SOSG and C-dots-Ce6 (1 μM) caused by the SO generated by C-dots-Ce6; (B) the changes of optical density at various peaks (256, 402, and 653 nm) as the function of laser irradiation time; (C) fluorescence emission spectra of C-dots-Ce6 in SOSG solution with the increase of the laser irradiation time; (D) the changes of fluorescence intensity at the characteristic peak of SOSG (530 nm) as a function of laser irradiation time. The concentration of Ce6 and C-dots-Ce6 is fixed at 1 μM. The mixture solutions were irradiated with a 671 nm laser (10 mW/cm^2). SOSG was dissolved in water containing 2% methanol with the final concentration of 2.5 μM. SOSG fluorescence emission was produced using an excitation wavelength of 494 nm.

Figure 4.
(A–C) Subcellular localization of C-dots-Ce6, monitored by fluorescence imaging using an upright Olympus IX71 optical microscope integrated with a CRi Nuance multispectral imaging system. MGC803 cells were incubated with C-dots-Ce6 at a concentration of 10 μM for 2 h at 37 °C (The scale bar is 25 μm); (D) MGC803 cells viability at different concentrations of Ce6 and C-dots-Ce6 for 24 h at 37 °C with or without irradiation for 3 min with a 671 nm laser (30 mW/cm^2). (P < 0.05 for other groups versus C-dots-Ce6 + laser group) (E, F) Trypan blue staining images of MGC803 cells incubated with C-dots-Ce6 at a concentration of 10 μM for 24 h at 37 °C prior to irradiation for 3 min with a 671 nm laser (30 mW/cm^2), (E) MGC803 cells on the laser spot, (F) MGC803 cells on the center of the laser spot (The scale bar is 100 μm).

Figure 5.
(A) Real-time *in vivo* NIR fluorescence images after intravenous injection of C-dots-Ce6 in nude mice at different time points; (B) *ex vivo* images of mice tissues (from top to bottom: heart, liver, spleen, lung, kidneys, tumor); (C) the average fluorescence intensities from the tumor area at 24 h post-injection (n = 5); (D) MGC803 tumor growth curves after various treatments (n = 5). (*, $P < 0.05$ for other groups versus C-dots-Ce6 + laser group)
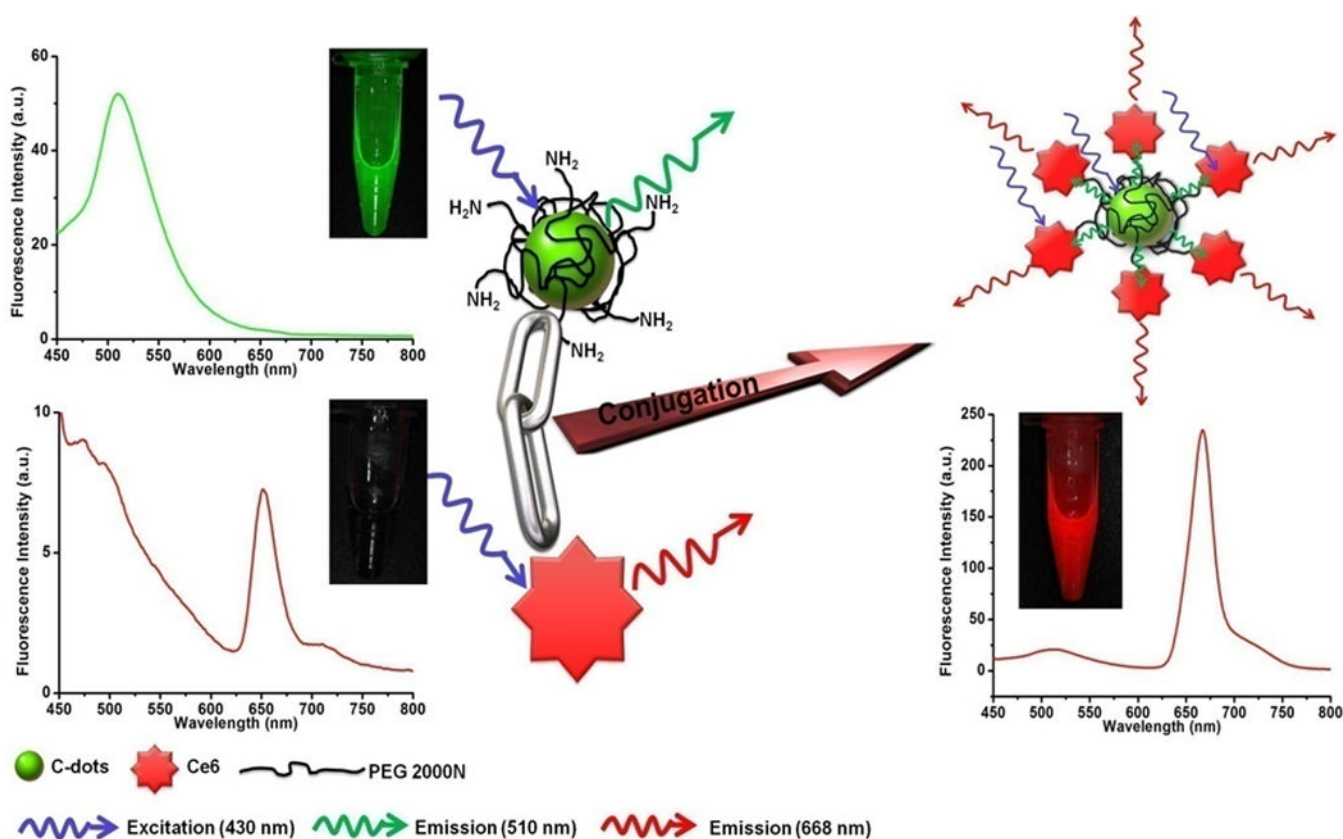
Scheme 1.
Förster (fluorescence) resonance energy transfer (FRET) process between C-dots and Ce6.